

Article

Towards Room Temperature Phase Transition of W-Doped VO₂ Thin Films Deposited by Pulsed Laser Deposition: Thermochromic, Surface, and Structural Analysis

Yannick Bleu ^{1,*} , Florent Bourquard ¹, Vincent Barnier ² , Anne-Sophie Loir ¹ , Florence Garrelie ¹ 
and Christophe Donnet ¹ 

¹ Université de Lyon, Université Jean Monnet-Saint-Étienne, CNRS, Institut d'Optique Graduate School, Laboratoire Hubert Curien, UMR 5516, F-42023 Saint-Etienne, France

² Mines Saint-Etienne, Université de Lyon, CNRS, UMR 5307 LGE, Centre SMS, F-42023 Saint-Etienne, France

* Correspondence: yannick.bleu@univ-st-etienne.fr

Abstract: Vanadium dioxide (VO₂) with an insulator-to-metal (IMT) transition (~68 °C) is considered a very attractive thermochromic material for smart window applications. Indeed, tailoring and understanding the thermochromic and surface properties at lower temperatures can enable room-temperature applications. The effect of W doping on the thermochromic, surface, and nanostructure properties of VO₂ thin film was investigated in the present proof. W-doped VO₂ thin films with different W contents were deposited by pulsed laser deposition (PLD) using V/W (+O₂) and V₂O₅/W multilayers. Rapid thermal annealing at 400–450 °C under oxygen flow was performed to crystallize the as-deposited films. The thermochromic, surface chemistry, structural, and morphological properties of the thin films obtained were investigated. The results showed that the V⁵⁺ was more surface sensitive and W distribution was homogeneous in all samples. Moreover, the V₂O₅ acted as a W diffusion barrier during the annealing stage, whereas the V+O₂ environment favored W surface diffusion. The phase transition temperature gradually decreased with increasing W content with a high efficiency of −26 °C per at. % W. For the highest doping concentration of 1.7 at. %, VO₂ showed room-temperature transition (26 °C) with high luminous transmittance (62%), indicating great potential for optical applications.

Keywords: vanadium dioxide; W doping; phase transition temperature; luminous transmittance; ARXPS



Citation: Bleu, Y.; Bourquard, F.; Barnier, V.; Loir, A.-S.; Garrelie, F.; Donnet, C. Towards Room Temperature Phase Transition of W-Doped VO₂ Thin Films Deposited by Pulsed Laser Deposition: Thermochromic, Surface, and Structural Analysis. *Materials* **2023**, *16*, 461. <https://doi.org/10.3390/ma16010461>

Academic Editor: Gueorgui Gueorguiev

Received: 5 December 2022

Revised: 21 December 2022

Accepted: 30 December 2022

Published: 3 January 2023



Copyright: © 2023 by the authors. Licensee MDPI, Basel, Switzerland. This article is an open access article distributed under the terms and conditions of the Creative Commons Attribution (CC BY) license (<https://creativecommons.org/licenses/by/4.0/>).

1. Introduction

VO₂ has the closest phase transition to room temperature of any the thermochromic oxide materials and has consequently been extensively studied for a variety of applications including electronic switches, smart windows, memory devices, RF microwave switches, and terahertz metamaterial devices [1–5]. Indeed, VO₂ enables insulator-to-metal transition (IMT) as well as transition from a monoclinic (M1) to a rutile structure (R) at around 68 °C [6]. However, the phase transition temperature of pristine VO₂ thin films is too high for room temperature applications. To meet the demand for a broad range of room temperature applications, considerable efforts have been made to reduce the phase transition temperature. One way to do so is replacing V⁴⁺ ions by metal ions with higher valences such as W⁶⁺, Nb⁵⁺, and Mo⁶⁺ [7–10], among which W has been considered one of the most effective dopants. Interestingly, the doping of W into the VO₂ matrix affects the transition characteristics. The substitutional doping of the W⁶⁺ to replace V⁴⁺ has been shown to lead to a remarkable reduction in the phase transition temperature, i.e., 20–28 °C per W at. % [7,10–14]. VO₂-based thin films can be synthesized using several techniques including sol-gel [15], magnetron sputtering [16,17], chemical vapor deposition [18], and pulsed laser deposition (PLD). However, there have been few reports on synthesizing W-doped VO₂

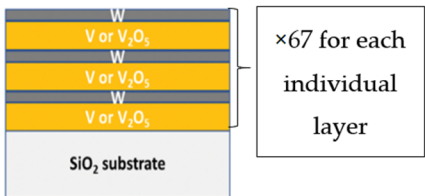
films using PLD [19–22], which is known to be a versatile method to control doping in thin films. Komal et al. [23] used mixed V_2O_3 and WO_3 pellets as targets for the PLD process and observed that the VO_2 doped with 1.5 at. % of W reduced the phase transition temperature towards room temperature (27 °C). Émond et al. [24] used PLD to prepare W-doped VO_2 films with a phase transition temperature of 36 °C. Soltani et al. [25] manufactured 1.6 at. % W-doped VO_2 thin films using a W-doped vanadium oxide target. The phase transition temperature was about 36 °C and all-optical switching was demonstrated at a telecommunication wavelength of 1.55 μm . S. S. Majid et al. [26] used a W-doped target and obtained W-doped VO_2 films with a significantly lower phase transition temperature (~ 19 °C for 1.3% W) by stabilizing the metallic rutile phase R. All these studies demonstrate that PLD is a versatile method capable of tuning the properties of VO_2 . However, they used either a target mixture of tungsten and vanadium oxide or a co-ablation process and mainly focused on reducing the phase transition temperature. In the present work, an innovative method to synthesize W-doped VO_2 thin films using pulsed laser deposition is proposed. This method consists in fabricating multilayers composed of V/W (+ O_2) and V_2O_5 /W bilayers, followed by rapid thermal annealing to allow both crystallization of VO_2 and the diffusion of W through the VO_2 layers to synthesize homogeneous W-doped VO_2 thin films. The main advantage of this process over co-ablation deposition is its repeatability. Indeed, co-ablation can cause problems of thickness and of non-homogeneous composition as well as contamination between the targets. In addition to the synthesis process, this work not only aims to reduce the phase transition temperature but also to improve our understanding of the surface chemistry of W-doped films. For the latter, angle-resolved X-ray photoelectron spectroscopy (ARXPS), which is rarely used in VO_2 -reported studies, was used to measure the concentration of vanadium, the depth of tungsten oxidation, as well as to assess their depth distribution.

2. Materials and Methods

2.1. Synthesis of W-Doped VO_2 Thin Films Using Pulsed Laser Deposition

W-doped VO_2 thin films were synthesized by rapid thermal annealing of multilayers composed of VO_x /W bilayers as illustrated in the figure inserted in Table 1. The bilayers were deposited on fused silica substrates using pulsed laser deposition (PLD) at room temperature. The PLD chamber was evacuated to a background pressure of 2×10^{-7} mbar. Three types of targets were used in the investigation: Vanadium (V), Vanadium pentoxide (V_2O_5), and Tungsten (W), all at 99.9% purity. A KrF excimer laser (wavelength 248 nm, repetition rate 10 Hz, fluence 13 J/cm²) was used to ablate the targets. The target/substrate distance was 5 cm. The laser beam was oriented with an angle of 45° to the target. For the W-doped VO_x using metallic vanadium as a precursor, the oxygen pressure inside the deposition chamber was 1×10^{-2} mbar when ultrapure O_2 was used. For the W-doped VO_x using the V_2O_5 target, ablation was performed without oxygen gas. During the deposition process, the targets were rotated to enable uniform ablation. For all depositions, the deposition rate obtained by profilometry was around 6.3 nm/min for V+ O_2 , 6.4 nm/min for V_2O_5 , and 1.37 nm/min for W. The alternative ablation sequences of V_2O_5 (or V in O_2) and W were adjusted to obtain three multilayers (A, B, C) with different W contents to obtain three W-doped VO_x thin films with a similar total thickness of 20 nm (Table 1).

Table 1. Condition of deposited multilayers using pulsed laser deposition. The ablated thickness per layer and the number of individual layers were adjusted to obtain three different W contents (next investigated using XPS).

			
	Sample A	Sample B	Sample C
V ablated thickness per layer (nm)	/	/	0.283
V ₂ O ₅ ablated thickness per layer (nm)	0.283	0.270	/
W ablated thickness per layer (nm)	0.015	0.03	0.015
Number of VO _x and W layers	67	67	67
Total thickness (nm)	20	20	20

The rapid thermal annealing process was performed using an RTP furnace (AS-One RTP system from Annealsys, Montpellier, France). For samples A and B, the annealing temperature was 400 °C for 120 s, while for sample C, the annealing temperature was 450 °C for 60 s. The time of rapid thermal annealing was adjusted from preliminary experiments, depending on the two different precursors, to ensure the observation of the thermochromic transition in both cases. All the annealing processes were carried out at an oxygen partial pressure of 1 mbar and a 50 sccm flow. The heating rate was 5 °C/s and the cooling was natural. The annealing chamber was evacuated to a 1×10^{-2} mbar before the oxygen was introduced. Undoped VO₂ thin films were obtained using a similar process for the purpose of comparison.

2.2. Characterization of the Undoped VO₂ and W-Doped VO₂ Films

The composition and dopant profile were investigated using XPS analysis using a Thermo VG Theta probe spectrometer (Thermo Fisher Scientific, Invitrogen, Waltham, MA, USA) with a focused monochromatic AlK α source ($h\nu = 1486.68$ eV, 400 μ m spot size) and photoelectrons were collected using a concentric hemispherical analyzer. A constant ΔE mode and a 2D channel plate detector (Thermo Fisher Scientific, Invitrogen, Waltham, MA, USA) were used. The energy scale was calibrated with sputter-cleaned pure reference samples of Au, Ag, and Cu such that Au4f_{7/2}, Ag3d_{5/2}, and Cu3p_{3/2} were positioned at binding energies of 83.98, 386.26, and 932.67 eV, respectively. Angle-resolved XPS analyses were performed thanks to the ability of the spectrometer to simultaneously collect several photoelectron emission angles in the acceptance range of 60° without tilting the sample. Charge neutralization was applied during analysis. High-resolution spectra (i.e., O1s-V2p, V3p-W4f) were fitted using AVANTAGE software version 5.9 by Thermo Fisher Scientific. The structure of the films was analyzed by Raman analysis (Jobin-Yvon ARAMIS) using a Helium-Neon laser source (Horiba Jobin Yvon, Gières, France) at an excitation wavelength of 633 nm, a laser power of 0.1 mW, focused with a 100 \times objective, consistent with a spot diameter of less than 1 mm. Atomic force microscopy (AFM) (Icon BRUKER, Berlin, Germany) and scanning electron microscopy (SEM) (JEOL IT 800 SHL, Tokyo, Japan) were used to analyze the topography, roughness, and morphology of the films. The thermochromic properties of the films were measured by collecting the transmittance in a temperature range between 15 and 100 °C using a fiber optic spectrometer (Ocean Insight, Duiven, The Netherlands) equipped with handmade heating units in the visible (400–800 nm) and IR (900–2500 nm) wavelength ranges. For the undoped and W-

doped VO₂ thin films, the integrated luminous transmittance (T_{lum} , 380–780 nm) and solar modulation efficiency (T_{sol} , 300–2500 nm) were deduced from the following equation:

$$T_{lum, sol} = \left(\int \varphi_{lum, sol}(\lambda) T(\lambda) d\lambda \right) / \left(\int \varphi_{lum, sol}(\lambda) d\lambda \right) \quad (1)$$

where $T(\lambda)$ is film transmittance at wavelength (λ), $\varphi_{lum}(\lambda)$ is the standard luminous efficiency depending on the photopic vision of human eye, $\varphi_{sol}(\lambda)$ is the solar irradiance spectrum (air mass 1.5) corresponding to the sun at an angle of 37° to the horizon [23]. ΔT_{sol} is obtained from $\Delta T_{sol} = T_{sol}(15^\circ\text{C}) - T_{sol}(100^\circ\text{C})$ and $T_{lum} = (T_{lum}(15^\circ\text{C}) + T_{lum}(100^\circ\text{C}))/2$.

3. Results and Discussion

3.1. Thermochromic Properties

To investigate the influence of W-doping on thermochromic properties, the transmittance of the samples during a heating and cooling phase were recorded and plotted the hysteresis loops of undoped and W-doped thin films.

Figure 1a shows the hysteresis loop produced by plotting the temperature dependence of transmittance of undoped and W-doped VO₂ thin films at a fixed wavelength of 1500 nm. The switching temperatures during heating ($T_{t,h}$) and cooling ($T_{t,c}$) were determined from the half-value width of each curve and the average temperature of commutation (T_t) representative of thermochromic behavior was defined as $T_t = (T_{t,h} + T_{t,c})/2$. Both undoped VO₂ films had a phase transition temperature T_t of 70–71 °C (quite similar whatever the precursors).

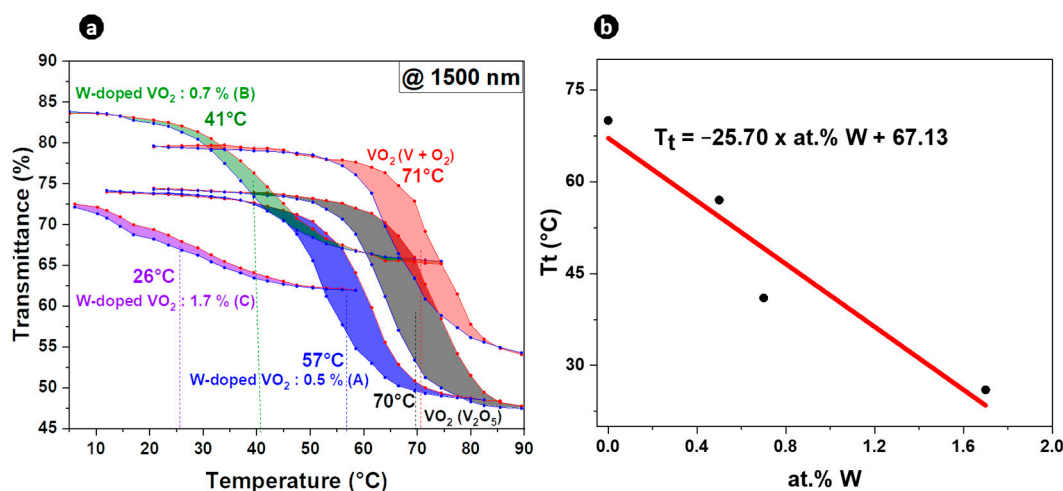


Figure 1. (a) Hysteresis loops derived from the temperature-dependent transmittance of the undoped and W-doped (A, B, and C) thin films at a wavelength of 1500 nm. (b) The correlation between the phase transition temperature T_t and W concentration.

The dependence of the phase transition temperature on the tungsten content was linear (Figure 1b). W doping significantly reduced T_t to $\sim -26^\circ\text{C}$ per at. % W, as shown in Figure 1b, which is in line with reported values of ~ 20 – 28°C per at. % W [7,12–14]. The T_t reduction mechanism of the W-doped VO₂ can be ascribed to free electron carriers generation [27] as well as to the extra strain resulting from the atom replacement of V⁴⁺ by W⁶⁺. This induced high symmetry around the W atom, implying transformation into a rutile structure [28,29], which was subsequently corroborated by Raman analysis.

Hysteresis behavior is another important thermochromic parameter of VO₂-based thin films. The hysteresis loop width gradually narrowed from 11 °C for the VO₂ film to 4 °C for the film doped with 1.7 at. % W, as can be seen in Figure 2a. This illustrates that the W dopant not only reduces the transition temperature but also reduces the width of the

hysteresis loop. Previous studies suggested that ΔT is closely linked to the grain size, lattice stress, impurity phase, and crystallinity of VO_2 film [30,31]. Structural defects induced by W doping act as nucleation sites of the phase transition [32,33]. Therefore, the activation energy of the phase transition would be reduced, with a decrease in hysteresis width. The result is promising, as narrow hysteresis loops are required to create devices with rapid commutations.

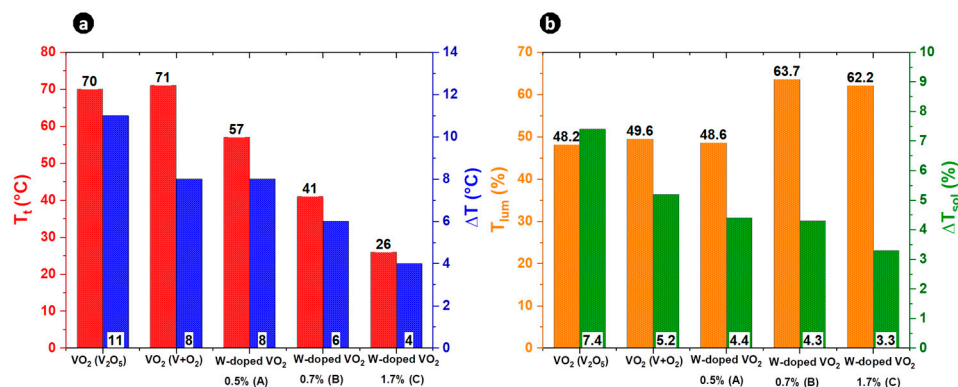


Figure 2. (a) Phase transition temperature (red) and hysteresis width (blue) for undoped and W-doped VO_2 thin films. (b) The corresponding luminous transmittance (T_{lum} , orange) and the solar modulation ability (ΔT_{sol} , in green) values.

Moreover, the luminous transmittance (T_{lum}) and the solar modulation ability (ΔT_{sol}) are plotted in Figure 2b. Compared to undoped VO_2 thin films, the luminous transmittance of the W-doped VO_2 thin films was higher. Indeed, T_{lum} increased with increasing W content. The luminous transmittance of the W-rich sample was 62.2%, a rather very good performance for W-doped VO_2 thin films. In the literature, the luminous transmittance of VO_2 after W-doping usually either remained unchanged or decreased, as reported in Table 2. In the present study, our W-doped VO_2 thin films had higher T_{lum} . Further investigations would be necessary to identify the exact origin of such a significant increase of T_{lum} at the two highest W contents. The solar modulation ability ΔT_{sol} decreased gradually with increasing W content. This is consistent with the results of previous works [34,35], in which ΔT_{sol} decreased with increasing W content. The variation of ΔT_{sol} depending on W content is in good agreement with the variation of T_t . Two explanations are possible: the incorporation of W induces a destabilization of VO_2 (M) lattice, and reduces the phase transition temperature. On the other hand, too much W doping leads to an excess of free electrons, thereby deteriorating the phase transition property [36]. Overall, as shown in Table 2, our W-doped VO_2 thin films outperformed other reported works on W-doped VO_2 using different synthesis methods in terms of reducing T_t and improving luminous transmittance.

Table 2. Comparison of some of the W-doped VO_2 reported works on thermochromic parameters including T_t , ΔT , T_{lum} , and ΔT_{sol} , with those of our present study. The terms « unchanged, increased, decreased » correspond to changes in the T_{lum} and ΔT_{sol} values of W-doped VO_2 compared to those of undoped VO_2 .

W (at. %)	T_t (°C)	ΔT (°C)	T_{lum}	ΔT_{sol}	Process	Structural Form	Ref.
0.14	64	6.8	Unchanged	Decreased	Electron beam evaporation	Thin film	[11]
2	28	15	Unchanged	Decreased	Spin coating	Thin film	[37]
0.4	43	/	Increased	Decreased	Hydrothermal	Mesoporous film	[38]

Table 2. Cont.

W (at. %)	T _t (°C)	ΔT (°C)	T _{lum}	ΔT _{sol}	Process	Structural Form	Ref.
0.8	36	20.5	Decreased	Decreased	Hydrothermal	Nanoparticles	[39]
3	44.4	18.4	Increased	Increased	Spin coating	Coating	[40]
2	43	/	Decreased	Decreased	Microemulsion technology	Nanostructure	[41]
1.3	55	/	Decreased	Decreased	Magnetron sputtering	Thin film	[42]
1.3	17.5	25.1	Increased	Decreased	Hydrothermal	Nanoparticle	[43]
0.7	41	6	Increased	Decreased	PLD	Thin film	This work
1.7	26	4	Increased	Decreased	PLD	Thin film	This work

3.2. Surface Chemistry Analysis: Composition and Depth Distribution

To analyze the surface chemistry, the high-resolution XPS spectra of V 2p and W 4d core-levels of W-doped VO_x (as-deposited) and W-doped VO₂ (after annealing) thin films are shown in Figure 3a,b, respectively.

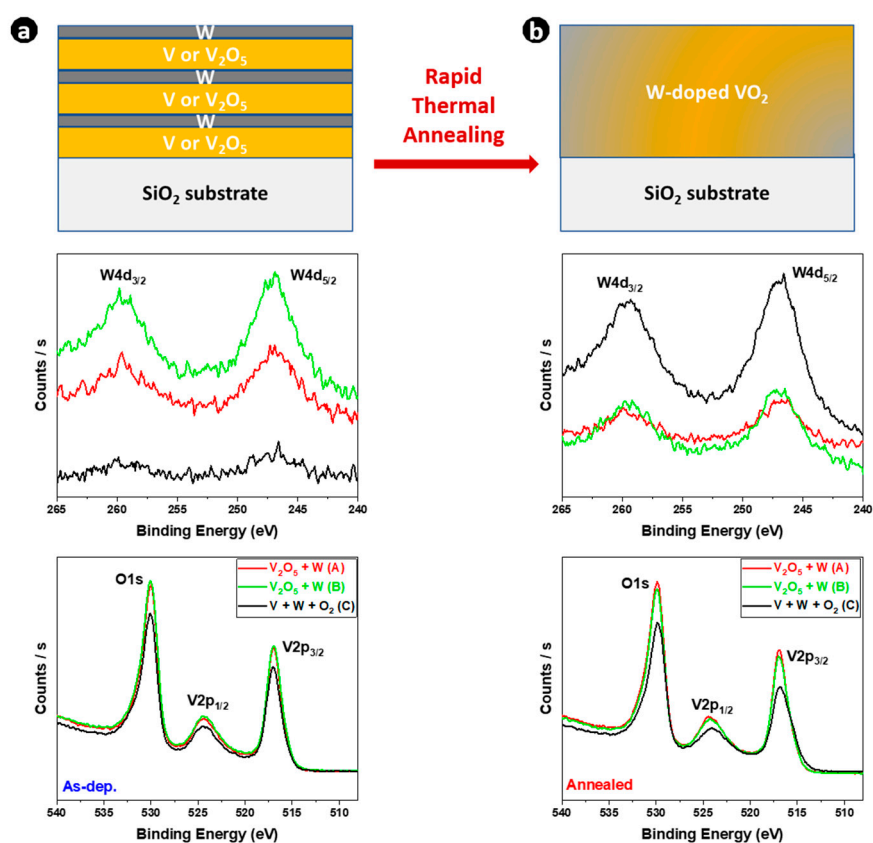


Figure 3. V 2p and W 4d core-level XPS spectra of (a) W-doped VO_x as-deposited thin films, and (b) W-doped VO₂ thin films after rapid thermal annealing.

The W peaks of W 4d_{5/2} and W 4d_{3/2} were located at 246.8 and 259.8 eV, respectively, reflecting the + 6 oxidation state of W ions in both thin films [11,12,41,44]. The V 2p core-level was split into two regions, V 2p_{3/2} located at 516.9 eV and V 2p_{1/2} located around 524 eV [45,46], with the O1s located at 530 eV. The intensity of vanadium and oxygen peaks is not the same for all films, especially when the two deposition precursors V/W

(O₂) and V₂O₅/W are compared. Since the intensity of the tungsten peak differed from one sample to another, the W content differed. The presence of W can also be confirmed by its W 4f valence state [11]. The angle-resolved XPS spectra of W 4f core-levels at 23° and 68° of sample C are shown in Figure 2a after thermal annealing. Two strong peaks of W 4f core-level located at 34.7 eV and 36.9 eV were assigned to W 4f_{7/2} and W 4f_{5/2}, respectively. This revealed that W⁶⁺ cations were present in W-doped VO₂ thin films in line with previous reported work [47], and confirmed the successful W-doping of VO₂ thin films. Furthermore, the atomic concentrations of W were calculated based on the XPS spectra of V 3p and W 4f and the results of the quantification are shown in Figure 4b.

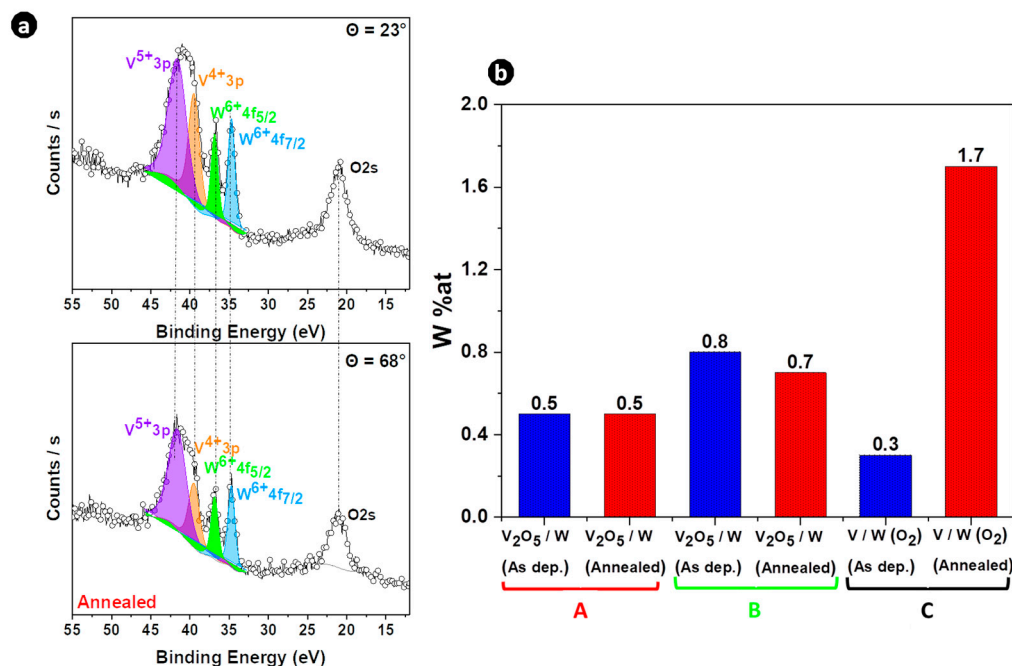


Figure 4. (a) Fitted ARXPS spectra of V 3p, W 4f, and O 2s core-levels for sample C after thermal annealing, at detection angles of 23° and 68°. (b) Quantification of W based on O 2s, W 4f, and V 3p peaks of the different samples before and after rapid thermal annealing.

Figure 4b reports W content in each sample before and after annealing. The annealing process did not significantly affect W content when the V₂O₅ target was used for W-doped VO₂ synthesis (samples A and B) because almost identical W contents were found consecutive to the annealing treatment. This suggests that V₂O₅ may act as a barrier to the surface diffusion of W. On the contrary, using the vanadium target, an increase in the W content after thermal annealing (sample C) was observed. This means that W diffused more towards the VO₂ surface during annealing and suggests that the V+O₂ environment favors the surface diffusion of W. Such an increase in W content during annealing was also recently reported by Ström et al. [48]. In their study, the W content in steel increased during thermal annealing and the modified composition was attributed to a near-surface effect. This might also be the case in our study, with surface diffusion of W towards the VO₂ surface during the annealing process.

For more insight into the depth distribution of W, Figure 5a,b show the dependence of the W⁶⁺ proportion as a function of the detection angle (23 to 76°) for all the samples before and after thermal annealing.

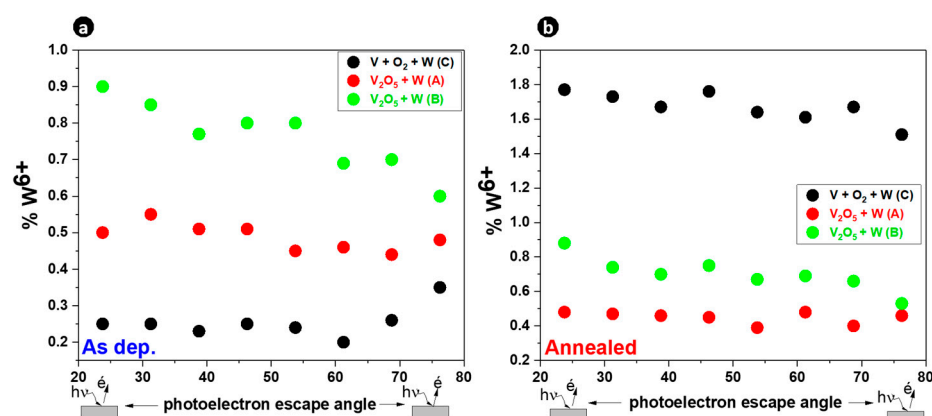


Figure 5. The proportion of W^{6+} based on V 3p, W 4f, and O 2s as a function of the ARXPS detection angle for all the samples (a) before thermal annealing and (b) after thermal annealing.

Similar W distribution between as-deposited and annealed films in samples A and B showed that the inter-diffusion between VO_x and W layers occurred at room temperature during deposition. In other words, the inter-diffusion process and the crystallization process occurred separately. Diffusion occurred during PLD deposition while crystallization occurred during the thermal annealing stage. Conversely, with sample C, the different W distribution between as-deposited and annealed films showed that the inter-diffusion between VO_x and W layers was not completed during PLD deposition, but was completed during the thermal annealing stage. This surface diffusion leads to an increase in W content toward the surface after thermal annealing. Therefore, along the first nanometers probed by ARXPS, sample C was richer in W after thermal annealing, while samples A and B had lower W contents. In addition, W distribution was almost constant with few discrepancies irrespective of the sample (before and after annealing), meaning that the W distribution was homogeneous in all the samples.

It is generally accepted that in addition to the doping element, the valence states of V can significantly affect the thermochromic characteristics of VO_2 -based thin films. Figure 6a,b show the high-resolution spectra of V 2p—O 1s recorded in XPS angle-resolved mode at two photoelectron take-off angles (23° and 68°) before and after thermal annealing for the W-rich sample (C). Deconvolution analysis of the V 2p_{3/2} and V 2p_{1/2} regions revealed two vanadium components in the samples, corresponding to V^{4+} and V^{5+} valence states: V^{4+} located at 516.1 eV for 2p_{3/2}, and 522.8 eV for 2p_{1/2} with V^{5+} centered at 517.1 eV for 2p_{3/2}, and 524.5 eV for 2p_{1/2} [45,46]. The binding energies of the peaks at 515.8 eV and 517.2 eV are close to those reported for VO_2 (515.7–516.2 eV) and V_2O_5 (516.9–517.2 eV), respectively [45,49,50]. There was no significant shift in the position of the peak in terms of the binding energy of the as-deposited and annealed samples. However, no difference in the intensity of the two oxidation states V^{4+} and V^{5+} was observed: the intensity of the V^{4+} oxidation state increased while that of V^{5+} decreased after thermal annealing. The O 1s peak is deconvoluted into two peaks, one corresponding to the O-C/O-H bond, which appeared at 531.2 eV due to surface contamination of the films. The other peak was due to the O-V bond located at 529.9 eV [51].

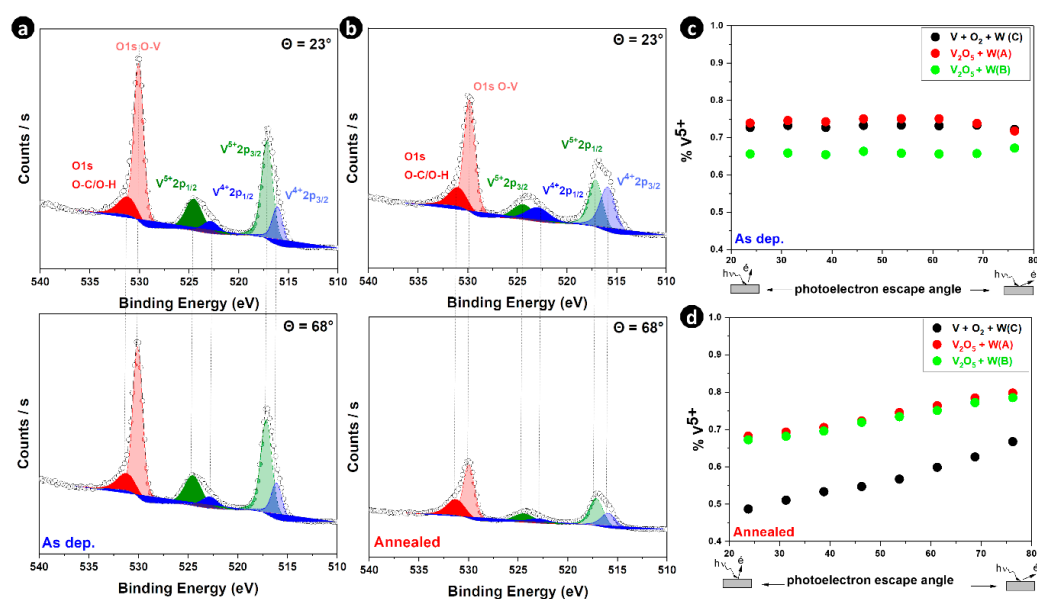


Figure 6. Fitted ARXPS spectra of V 2p and O 1s core-levels for sample C at detection angles of 23° and 68°, respectively, (a) before thermal annealing and (b) after thermal annealing. The concentration of the V⁵⁺ oxidation state of vanadium was obtained from the fitted spectra of the V 2p electrons as a function of the angle of detection in all the samples, (c) before thermal annealing and (d) after thermal annealing.

To investigate the depth distribution of the V⁵⁺ oxidation state of vanadium, the spectra of V 2p were measured at various detection angles ranging from 23° to 76° using angle-resolved X-ray photoelectron spectroscopy. Figure 6c,d shows the dependence of the concentration of the V⁵⁺ oxidation state as a function of the detection angle for all the samples before and after thermal annealing. It can be seen from Figure 6c that the angle dependence of V⁵⁺ oxidation state concentration is quite similar to that before thermal annealing, indicating homogeneous distribution of V⁵⁺ on the surface of all samples. After thermal annealing (Figure 5d), the proportion of the V⁵⁺ oxidation state increased with the increase in the detection angle in all samples. The results of angle-resolved measurements confirmed that the outer part of the W-doped VO₂ thin films was enriched in V⁵⁺, especially when the V₂O₅ target was used for the synthesis of W-doped VO₂ films and hence, that the other V⁴⁺ oxidation state is located in the inner region of the films. To summarize, sample C was poorer in V⁵⁺ and richer in W while samples A and B were richer in V⁵⁺ and poorer in W after thermal annealing.

3.3. Structural and Morphological Analysis

The structural change that occurred with W doping at room temperature was investigated using Raman analysis.

Figure 7 shows the Raman spectra of the undoped and W-doped thin films at room temperature. The two undoped VO₂ films (black and red curves in Figure 7) had typical peaks at 143 (Ag), 192 (Ag), 222 (Ag), 262 (Bg), 306 (Ag), 338 (Ag), 389 (Ag), 441 (Bg), 498 (Ag), and 617 (Ag) cm^{−1}, corresponding to the monoclinic VO₂ (M1) phase [52–54]. No vibration peak of V₂O₅ was observed, perhaps due to the low concentration of V₂O₅ resulting in weaker molecular vibration. Concerning the W-doped VO₂ films, a decrease in the intensities of the Raman active modes (low-frequency and high-frequency mode) and broadening of the peaks with an increase on the percentage of W doping were observed. This can be explained by the fact that W doping starts to favor a more symmetric rutile structure. A similar effect has already been reported for W-doped VO₂ films [23,55] and Nb-doped VO₂ films [56]. Moreover, the 617 (Ag) cm^{−1} phonon mode was slightly upshifted and broadened as well as being reduced in intensity with W doping up to 625 cm^{−1}.

(green curve), indicating a distorted M1 phase and the nucleation of rutile domains at this stage [57]. In the W-rich sample (1.7 at. % W), some modes started to disappear (purple curve), indicating the beginning of the metallic rutile phase as observed in the above-mentioned analysis of the phase transition temperature.

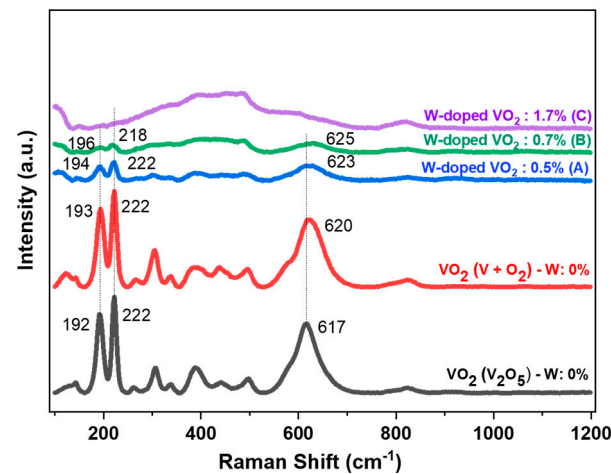


Figure 7. Raman spectra of undoped and W-doped VO₂ (samples A, B, and C) thin films.

Changes in the surface morphology and variations in the surface roughness of the undoped and W-doped VO₂ thin films were investigated by SEM and AFM, respectively. Regarding the thin films obtained using V+O₂ deposition, the surface morphology of undoped film (Figure 8a) was flat with trace-like cracks whereas with W doping, the surface of the film contained holes resembling pores. The surface morphology of the films deposited from the V₂O₅ target was uniform, dense, and compact, the undoped film being slightly smoother than the W-doped film. The difference in morphology between undoped and W-doped VO₂ films can be attributed to the general regularity observed in solid solution formation: an increase in the number of constituents can play a role in the crystallization of the films [58,59]. AFM scanning maps of the films obtained from V+O₂ exhibited a slight decrease in the root mean square (RMS) from the undoped to W-doped VO₂ films. The RMS of the W-doped VO₂ film obtained from V₂O₅, was slightly higher than that of the undoped film. However, the low RMS values indicate that our VO₂-based thin films are extraordinarily smooth with improved quality compared to those obtained using other synthesis methods [60,61].

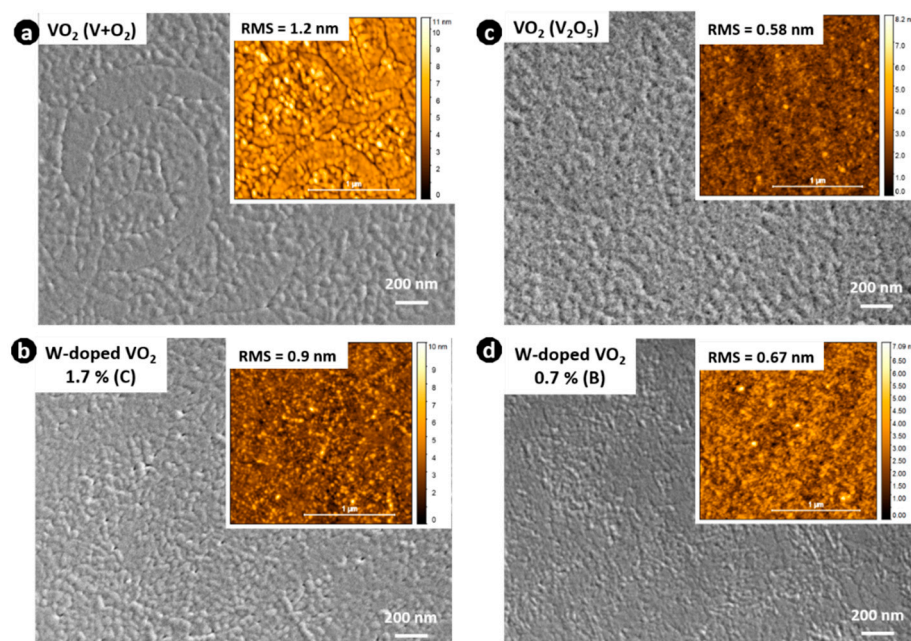


Figure 8. Top-view SEM micrographs of the obtained thin films after rapid thermal annealing (a) VO_2 thin film obtained from $\text{V}+\text{O}_2$. (b) W-doped VO_2 (1.7 at. % W, sample C). (c) VO_2 thin film obtained from V_2O_5 . (d) W-doped VO_2 thin film (0.7 at. % W, sample B). The inserts correspond to the AFM images.

4. Conclusions

An innovative PLD method was developed to synthesize smooth W-doped thin films using $\text{V}/\text{W} (+\text{O}_2)$ and $\text{V}_2\text{O}_5/\text{W}$ multilayers with subsequent post-rapid thermal annealing. Our results revealed that the inter-diffusion between the W and VO_x layers was completed during the PLD deposition process at room temperature when the V_2O_5 target was used, whereas when the $\text{V}+\text{O}_2$ source was used, inter-diffusion between the W and VO_x layers was completed during the thermal annealing stage. Therefore, the V_2O_5 acted as a W diffusion barrier, while the $\text{V}+\text{O}_2$ environment favored surface diffusion of W during the annealing stage. These findings also show that the V^{5+} is more surface sensitive and that the distribution of W on the surface of the samples is homogeneous. Furthermore, as expected, W doping leads to a sharp decrease in the VO_2 IMT by a highly efficient reduction of the phase transition temperature -26°C per at. % W. With W-doping of 1.7 at. %, the concentration of V^{5+} decreased, and the transition temperature of VO_2 dropped to room temperature (26°C), accompanied by a high luminous transmittance (62%) while retaining a narrow hysteresis width. These very good thermochromic properties have high potential in the application of smart windows and optical devices based on thermochromic switching behavior.

Author Contributions: Conceptualization, C.D. and F.G.; Methodology, F.B. and A.-S.L.; Investigation, Y.B. and V.B.; Writing—Original Draft Preparation, Y.B.; Writing—Review & Editing, Y.B. and C.D.; Visualization, C.D.; Supervision, C.D., F.B. and F.G.; Project Administration, F.B. and C.D. All authors have read and agreed to the published version of the manuscript.

Funding: This research was funded by the LABEX MANUTECH-SISE (ANR-10-LABX-0075) of Université de Lyon.

Data Availability Statement: Data is available from the corresponding author upon reasonable request.

Acknowledgments: This work was supported by the LABEX MANUTECH-SISE (ANR-10-LABX-0075) of Université de Lyon, in the framework of Plan France 2030 operated by the French National Research Agency (ANR).

Conflicts of Interest: The authors declare no conflict of interest.

References

- Chen, S.; Wang, Z.; Ren, H.; Chen, Y.; Yan, W.; Wang, C.; Li, B.; Jiang, J.; Zou, C. Gate-Controlled VO₂ Phase Transition for High-Performance Smart Windows. *Sci. Adv.* **2019**, *5*, eaav6815. [\[CrossRef\]](#) [\[PubMed\]](#)
- Mizsei, J.; Lappalainen, J.; Pohl, L. Active Thermal-Electronic Devices Based on Heat-Sensitive Metal-Insulator-Transition Resistor Elements. *Sens. Actuators A Phys.* **2017**, *267*, 14–20. [\[CrossRef\]](#)
- Beaumont, A.; Leroy, J.; Orlianges, J.-C.; Crunteanu, A. Current-Induced Electrical Self-Oscillations across out-of-Plane Threshold Switches Based on VO₂ Layers Integrated in Crossbars Geometry. *J. Appl. Phys.* **2014**, *115*, 154502. [\[CrossRef\]](#)
- Vardi, N.; Anouchi, E.; Yamin, T.; Middey, S.; Kareev, M.; Chakhalian, J.; Dubi, Y.; Sharoni, A. Ramp-Reversal Memory and Phase-Boundary Scarring in Transition Metal Oxides. *Adv. Mater.* **2017**, *29*, 1605029. [\[CrossRef\]](#) [\[PubMed\]](#)
- Lee, J.; Lee, D.; Cho, S.J.; Seo, J.-H.; Liu, D.; Eom, C.-B.; Ma, Z. Epitaxial VO₂ Thin Film-Based Radio-Frequency Switches with Thermal Activation. *Appl. Phys. Lett.* **2017**, *111*, 063110. [\[CrossRef\]](#)
- Ji, Y.D.; Pan, T.S.; Bi, Z.; Liang, W.Z.; Zhang, Y.; Zeng, H.Z.; Wen, Q.Y.; Zhang, H.W.; Chen, C.L.; Jia, Q.X.; et al. Epitaxial Growth and Metal-Insulator Transition of Vanadium Oxide Thin Films with Controllable Phases. *Appl. Phys. Lett.* **2012**, *101*, 071902. [\[CrossRef\]](#)
- Burkhardt, W.; Christmann, T.; Meyer, B.K.; Niessner, W.; Schalch, D.; Scharmann, A. W- and F-Doped VO₂ Films Studied by Photoelectron Spectrometry. *Thin Solid Film.* **1999**, *345*, 229–235. [\[CrossRef\]](#)
- Guan, S.; Souquet-Basiège, M.; Toulemonde, O.; Denux, D.; Penin, N.; Gaudon, M.; Rougier, A. Toward Room-Temperature Thermochromism of VO₂ by Nb Doping: Magnetic Investigations. *Chem. Mater.* **2019**, *31*, 9819–9830. [\[CrossRef\]](#)
- Khan, G.R.; Asokan, K.; Ahmad, B. Room Temperature Tunability of Mo-Doped VO₂ Nanofilms across Semiconductor to Metal Phase Transition. *Thin Solid Film.* **2017**, *625*, 155–162. [\[CrossRef\]](#)
- Piccirillo, C.; Binions, R.; Parkin, I.P. Nb-Doped VO₂ Thin Films Prepared by Aerosol-Assisted Chemical Vapour Deposition. *Eur. J. Inorg. Chem.* **2007**, *2007*, 4050–4055. [\[CrossRef\]](#)
- Chen, S.-E.; Lu, H.-H.; Brahma, S.; Huang, J.-L. Effects of Annealing on Thermochromic Properties of W-Doped Vanadium Dioxide Thin Films Deposited by Electron Beam Evaporation. *Thin Solid Film.* **2017**, *644*, 52–56. [\[CrossRef\]](#)
- Romanyuk, A.; Steiner, R.; Marot, L.; Oelhafen, P. Temperature-Induced Metal–Semiconductor Transition in W-Doped VO₂ Films Studied by Photoelectron Spectroscopy. *Sol. Energy Mater. Sol. Cells* **2007**, *91*, 1831–1835. [\[CrossRef\]](#)
- Tang, C.; Georgopoulos, P.; Fine, M.E.; Cohen, J.B.; Nygren, M.; Knapp, G.S.; Aldred, A. Local Atomic and Electronic Arrangements in W_xV_{1-x}O₂. *Phys. Rev. B* **1985**, *31*, 1000–1011. [\[CrossRef\]](#) [\[PubMed\]](#)
- Jin, P.; Tazawa, M.; Ikeyama, M.; Tanemura, S.; Macák, K.; Wang, X.; Olafsson, S.; Helmersson, U. Growth and Characterization of Epitaxial Films of Tungsten-Doped Vanadium Oxides on Sapphire (110) by Reactive Magnetron Sputtering. *J. Vac. Sci. Technol. A* **1999**, *17*, 1817–1821. [\[CrossRef\]](#)
- Lee, Y.W.; Kim, B.-J.; Lim, J.-W.; Yun, S.J.; Choi, S.; Chae, B.-G.; Kim, G.; Kim, H.-T. Metal-Insulator Transition-Induced Electrical Oscillation in Vanadium Dioxide Thin Film. *Appl. Phys. Lett.* **2008**, *92*, 162903. [\[CrossRef\]](#)
- Karaoglan-Bebek, G.; Hoque, M.N.F.; Holtz, M.; Fan, Z.; Bernussi, A.A. Continuous Tuning of W-Doped VO₂ Optical Properties for Terahertz Analog Applications. *Appl. Phys. Lett.* **2014**, *105*, 201902. [\[CrossRef\]](#)
- Yu, S.; Wang, S.; Lu, M.; Zuo, L. A Metal-Insulator Transition Study of VO₂ Thin Films Grown on Sapphire Substrates. *J. Appl. Phys.* **2017**, *122*, 235102. [\[CrossRef\]](#)
- Sahana, M.B.; Subbanna, G.N.; Shivashankar, S.A. Phase Transformation and Semiconductor-Metal Transition in Thin Films of VO₂ Deposited by Low-Pressure Metalorganic Chemical Vapor Deposition. *J. Appl. Phys.* **2002**, *92*, 6495–6504. [\[CrossRef\]](#)
- Ahmed, N.; Mahmood, R.; Umar, Z.A.; Liaqat, U.; ul Haq, M.A.; Ahmed, R.; Ahmad, P.; Raza, S.R.A.; Baig, M.A. Near Room Temperature, SMT and Visible Photo-Response in Pulsed Laser Deposited VO₂ (M1) Thin Films. *Phys. B Condens. Matter* **2022**, *635*, 413841. [\[CrossRef\]](#)
- Umar, Z.A.; Ahmed, N.; Ahmed, R.; Arshad, M.; Anwar-Ul-Haq, M.; Hussain, T.; Baig, M.A. Substrate Temperature Effects on the Structural, Compositional, and Electrical Properties of VO₂ Thin Films Deposited by Pulsed Laser Deposition. *Surf. Interface Anal.* **2018**, *50*, 297–303. [\[CrossRef\]](#)
- Bhardwaj, D.; Goswami, A.; Umarji, A.M. Synthesis of Phase Pure Vanadium Dioxide (VO₂) Thin Film by Reactive Pulsed Laser Deposition. *J. Appl. Phys.* **2018**, *124*, 135301. [\[CrossRef\]](#)
- Bleu, Y.; Bourquard, F.; Jamon, D.; Loir, A.-S.; Garrelie, F.; Donnet, C. Tailoring Thermochromic and Optical Properties of VO₂ Thin Films by Pulsed Laser Deposition Using Different Starting Routes. *Opt. Mater.* **2022**, *133*, 113004. [\[CrossRef\]](#)
- Mulchandani, K.; Soni, A.; Pathy, K.; Mavani, K.R. Structural Transformation and Tuning of Electronic Transitions by W-Doping in VO₂ Thin Films. *Superlattices Microstruct.* **2021**, *154*, 106883. [\[CrossRef\]](#)

24. Émond, N.; Ibrahim, A.; Torriess, B.; Hendaoui, A.; Al-Naib, I.; Ozaki, T.; Chaker, M. Impact of Tungsten Doping on the Dynamics of the Photo-Induced Insulator-Metal Phase Transition in VO₂ Thin Film Investigated by Optical Pump-Terahertz Probe Spectroscopy. *Appl. Phys. Lett.* **2017**, *111*, 092105. [\[CrossRef\]](#)
25. Soltani, M.; Chaker, M.; Haddad, E.; Kruzelecky, R.V.; Nikanpour, D. Optical Switching of Vanadium Dioxide Thin Films Deposited by Reactive Pulsed Laser Deposition. *J. Vac. Sci. Technol. A* **2004**, *22*, 859–864. [\[CrossRef\]](#)
26. Majid, S.S.; Sahu, S.R.; Ahad, A.; Dey, K.; Gautam, K.; Rahman, F.; Behera, P.; Deshpande, U.; Sathe, V.G.; Shukla, D.K. Role of V-V Dimerization in the Insulator-Metal Transition and Optical Transmittance of Pure and Doped VO₂ Thin Films. *Phys. Rev. B* **2020**, *101*, 014108. [\[CrossRef\]](#)
27. Goodenough, J.B. The Two Components of the Crystallographic Transition in VO₂. *J. Solid State Chem.* **1971**, *3*, 490–500. [\[CrossRef\]](#)
28. Asayesh-Ardakani, H.; Nie, A.; Marley, P.M.; Zhu, Y.; Phillips, P.J.; Singh, S.; Mashayek, F.; Sambandamurthy, G.; Low, K.; Klie, R.F.; et al. Atomic Origins of Monoclinic-Tetragonal (Rutile) Phase Transition in Doped VO₂ Nanowires. *Nano Lett.* **2015**, *15*, 7179–7188. [\[CrossRef\]](#)
29. Tan, X.; Yao, T.; Long, R.; Sun, Z.; Feng, Y.; Cheng, H.; Yuan, X.; Zhang, W.; Liu, Q.; Wu, C.; et al. Unraveling Metal-Insulator Transition Mechanism of VO₂ Triggered by Tungsten Doping. *Sci. Rep.* **2012**, *2*, 466. [\[CrossRef\]](#)
30. Zheng, T.; Sang, J.; Hua, Z.; Xu, L.; Xu, X.; Wang, C.; Wu, B. A Simple Method for Synthesizing VO₂ with Almost Coincident Hysteresis Loops on Si Substrate Containing TiO₂ Buffer Layer. *J. Alloys Compd.* **2021**, *865*, 158755. [\[CrossRef\]](#)
31. Suh, J.Y.; Lopez, R.; Feldman, L.C.; Haglund, R.F. Semiconductor to Metal Phase Transition in the Nucleation and Growth of VO₂ Nanoparticles and Thin Films. *J. Appl. Phys.* **2004**, *96*, 1209–1213. [\[CrossRef\]](#)
32. Jin, P.; Nakao, S.; Tanemura, S. Tungsten Doping into Vanadium Dioxide Thermochromic Films by High-Energy Ion Implantation and Thermal Annealing. *Thin Solid Film.* **1998**, *324*, 151–158. [\[CrossRef\]](#)
33. Lopez, R.; Haynes, T.E.; Boatner, L.A.; Feldman, L.C.; Haglund, R.F. Size Effects in the Structural Phase Transition of VO₂ Nanoparticles. *Phys. Rev. B* **2002**, *65*, 224113. [\[CrossRef\]](#)
34. Hu, L.; Tao, H.; Chen, G.; Pan, R.; Wan, M.; Xiong, D.; Zhao, X. Porous W-Doped VO₂ Films with Simultaneously Enhanced Visible Transparency and Thermochromic Properties. *J. Sol-Gel Sci. Technol.* **2016**, *77*, 85–93. [\[CrossRef\]](#)
35. Li, B.; Tian, S.; Tao, H.; Zhao, X. Tungsten Doped M-Phase VO₂ Mesoporous Nanocrystals with Enhanced Comprehensive Thermochromic Properties for Smart Windows. *Ceram. Int.* **2019**, *45*, 4342–4350. [\[CrossRef\]](#)
36. Shen, N.; Chen, S.; Shi, R.; Niu, S.; Amini, A.; Cheng, C. Phase Transition Hysteresis of Tungsten Doped VO₂ Synergistically Boosts the Function of Smart Windows in Ambient Conditions. *ACS Appl. Electron. Mater.* **2021**, *3*, 3648–3656. [\[CrossRef\]](#)
37. Zomaya, D.; Xu, W.Z.; Grohe, B.; Mittler, S.; Charpentier, P.A. W-Doped VO₂/PVP Coatings with Enhanced Thermochromic Performance. *Sol. Energy Mater. Sol. Cells* **2019**, *200*, 109900. [\[CrossRef\]](#)
38. Zou, J.; Chen, X.; Xiao, L. Phase Transition Performance Recovery of W-Doped VO₂ by Annealing Treatment. *Mater. Res. Express* **2018**, *5*, 065055. [\[CrossRef\]](#)
39. Dang, Y.; Zhao, L.; Liu, J. Preparation and Optical Properties of W-Doped VO₂/AZO Bilayer Composite Film. *Ceram. Int.* **2020**, *46*, 9079–9085. [\[CrossRef\]](#)
40. Zhang, L.; Xia, F.; Yao, J.; Zhu, T.; Xia, H.; Yang, G.; Liu, B.; Gao, Y. Facile Synthesis, Formation Mechanism and Thermochromic Properties of W-Doped VO₂ (M) Nanoparticles for Smart Window Applications. *J. Mater. Chem. C* **2020**, *8*, 13396–13404. [\[CrossRef\]](#)
41. Shen, N.; Chen, S.; Chen, Z.; Liu, X.; Cao, C.; Dong, B.; Luo, H.; Liu, J.; Gao, Y. The Synthesis and Performance of Zr-Doped and W-Zr-Codoped VO₂ Nanoparticles and Derived Flexible Foils. *J. Mater. Chem. A* **2014**, *2*, 15087–15093. [\[CrossRef\]](#)
42. Liang, Z.; Zhao, L.; Meng, W.; Zhong, C.; Wei, S.; Dong, B.; Xu, Z.; Wan, L.; Wang, S. Tungsten-Doped Vanadium Dioxide Thin Films as Smart Windows with Self-Cleaning and Energy-Saving Functions. *J. Alloys Compd.* **2017**, *694*, 124–131. [\[CrossRef\]](#)
43. Wang, S.; Wei, W.; Huang, T.; Yuan, M.; Yang, Y.; Yang, W.; Zhang, R.; Zhang, T.; Chen, Z.; Chen, X.; et al. Al-Doping-Induced VO₂ (B) Phase in VO₂ (M) Toward Smart Optical Thin Films with Modulated ΔT_{vis} and ΔT_c. *Adv. Eng. Mater.* **2019**, *21*, 1900947. [\[CrossRef\]](#)
44. Takami, H.; Kanki, T.; Ueda, S.; Kobayashi, K.; Tanaka, H. Electronic Structure of W-Doped VO₂ Thin Films with Giant Metal-Insulator Transition Investigated by Hard X-Ray Core-Level Photoemission Spectroscopy. *Appl. Phys. Express* **2010**, *3*, 063201. [\[CrossRef\]](#)
45. Sawatzky, G.A.; Post, D. X-Ray Photoelectron and Auger Spectroscopy Study of Some Vanadium Oxides. *Phys. Rev. B* **1979**, *20*, 1546–1555. [\[CrossRef\]](#)
46. Zhang, Z.; Gao, Y.; Chen, Z.; Du, J.; Cao, C.; Kang, L.; Luo, H. Thermochromic VO₂ Thin Films: Solution-Based Processing, Improved Optical Properties, and Lowered Phase Transformation Temperature. *Langmuir* **2010**, *26*, 10738–10744. [\[CrossRef\]](#)
47. Li, D.; Zhao, Z.; Wang, C.; Deng, S.; Yang, J.; Wang, X.; Li, J.; Zhao, Y.; Jin, H. Influence of the Charge Compensation Effect on the Metal-Insulator Transition of Mg-W Co-Doped VO₂. *Appl. Surf. Sci.* **2022**, *579*, 151990. [\[CrossRef\]](#)
48. Ström, P.; Primetzhofer, D. In-Situ Measurement of Diffusion and Surface Segregation of W and Ta in Bare and W-Coated EUROFER97 during Thermal Annealing. *Nucl. Mater. Energy* **2021**, *27*, 100979. [\[CrossRef\]](#)
49. Demeter, M.; Neumann, M.; Reichelt, W. Mixed-Valence Vanadium Oxides Studied by XPS. *Surf. Sci.* **2000**, *454–456*, 41–44. [\[CrossRef\]](#)
50. Silversmit, G.; Depla, D.; Poelman, H.; Marin, G.B.; De Gryse, R. Determination of the V2p XPS Binding Energies for Different Vanadium Oxidation States (V⁵⁺ to V⁰⁺). *J. Electron Spectrosc. Relat. Phenom.* **2004**, *135*, 167–175. [\[CrossRef\]](#)

51. Lee, D.; Kim, H.; Kim, J.W.; Lee, I.J.; Kim, Y.; Yun, H.-J.; Lee, J.; Park, S. Hydrogen Incorporation Induced the Octahedral Symmetry Variation in VO₂ Films. *Appl. Surf. Sci.* **2017**, *396*, 36–40. [[CrossRef](#)]
52. Shvets, P.; Dikaya, O.; Maksimova, K.; Goikhman, A. A Review of Raman Spectroscopy of Vanadium Oxides. *J. Raman Spectrosc.* **2019**, *50*, 1226–1244. [[CrossRef](#)]
53. Schilbe, P. Raman Scattering in VO₂. *Phys. B Condens. Matter* **2002**, *316–317*, 600–602. [[CrossRef](#)]
54. Srivastava, R.; Chase, L.L. Raman Spectrum of Semiconducting and Metallic VO₂. *Phys. Rev. Lett.* **1971**, *27*, 727–730. [[CrossRef](#)]
55. Gu, D.; Zhou, X.; Sun, Z.; Jiang, Y. Influence of Gadolinium-Doping on the Microstructures and Phase Transition Characteristics of VO₂ Thin Films. *J. Alloys Compd.* **2017**, *705*, 64–69. [[CrossRef](#)]
56. Ji, C.; Wu, Z.; Wu, X.; Feng, H.; Wang, J.; Huang, Z.; Zhou, H.; Yao, W.; Gou, J.; Jiang, Y. Optimization of Metal-to-Insulator Phase Transition Properties in Polycrystalline VO₂ Films for Terahertz Modulation Applications by Doping. *J. Mater. Chem. C* **2018**, *6*, 1722–1730. [[CrossRef](#)]
57. Whittaker, L.; Wu, T.-L.; Stabile, A.; Sambandamurthy, G.; Banerjee, S. Single-Nanowire Raman Microprobe Studies of Doping-, Temperature-, and Voltage-Induced Metal–Insulator Transitions of W_xV_{1–x}O₂ Nanowires. *ACS Nano* **2011**, *5*, 8861–8867. [[CrossRef](#)] [[PubMed](#)]
58. Liu, X.; Wang, S.-W.; Chen, F.; Yu, L.; Chen, X. Tuning Phase Transition Temperature of VO₂ Thin Films by Annealing Atmosphere. *J. Phys. D Appl. Phys.* **2015**, *48*, 265104. [[CrossRef](#)]
59. Zhao, Z.; Li, J.; Ling, C.; Zhao, X.; Zhao, Y.; Jin, H. Electric Field Driven Abnormal Increase in Conductivity of Tungsten-Doped VO₂ Nanofilms. *Thin Solid Film.* **2021**, *725*, 138643. [[CrossRef](#)]
60. Ivanov, A.V.; Tatarenko, A.Y.; Gorodetsky, A.A.; Makarevich, O.N.; Navarro-Cía, M.; Makarevich, A.M.; Kaul, A.R.; Eliseev, A.A.; Boytsova, O.V. Fabrication of Epitaxial W-Doped VO₂ Nanostructured Films for Terahertz Modulation Using the Solvothermal Process. *ACS Appl. Nano Mater.* **2021**, *4*, 10592–10600. [[CrossRef](#)]
61. Pan, G.; Yin, J.; Ji, K.; Li, X.; Cheng, X.; Jin, H.; Liu, J. Synthesis and Thermochromic Property Studies on W Doped VO₂ Films Fabricated by Sol-Gel Method. *Sci. Rep.* **2017**, *7*, 6132. [[CrossRef](#)] [[PubMed](#)]

Disclaimer/Publisher’s Note: The statements, opinions and data contained in all publications are solely those of the individual author(s) and contributor(s) and not of MDPI and/or the editor(s). MDPI and/or the editor(s) disclaim responsibility for any injury to people or property resulting from any ideas, methods, instructions or products referred to in the content.